Intrinsic Electron Beam Emittance from Metal Photocathodes: The Effect of the Electron Effective Mass

B. L. Rickman,[1,*] Joel A. Berger,[1] A. W. Nicholls,[2] and W. Andreas Schroeder[1]

[1]*Department of Physics, University of Illinois at Chicago, 845 W. Taylor Street, Chicago, Illinois 60607-7059, USA*

[2]*Research Resources Center, University of Illinois at Chicago, 845 W. Taylor Street, Chicago, Illinois 60607-7059, USA*

(Received 25 July 2013; published 4 December 2013)

A theoretical development of prior analyses, together with our solenoid scan measurements on eight planar metal photocathodes (Ag, Be, Cr, Cu, Mo, Sn, Ta, and W) and previous data on Mg [X. J. Wang, M. Babzien, R. Malone, and Z. Wu, in *Proceedings of LINAC2002, Gyeongju, Korea, 2002* (Pohang Accelerator Laboratory, Pohang, Korea, 2002), pp. 142–144.] indicate that the transverse momentum (and hence intrinsic emittance) of an electron beam is fundamentally dependent on the electron effective mass in the metal.

DOI: 10.1103/PhysRevLett.111.237401 PACS numbers: 85.60.Ha, 07.78.+s, 79.60.Bm, 81.05.Bx

Pulsed laser-driven electron guns are now becoming an integral part of modern scientific research instrumentation with uses ranging from ultrafast electron diffraction [1–3], through ultrafast and dynamic transmission electron microscopy (UTEM and DTEM, respectively) [4–6], to the front end of x-ray free electron lasers (XFELs) [7,8] and future compact pulsed x-ray sources [9]. Metals, due to their robustness (allowing operation at pressures of $>10^{-9}$ Torr) and near instantaneous response time, are a preferred photocathode material, especially for subpicosecond photoelectron guns. As electron optics continue to improve, the performance of scientific instruments with such ultrafast electron sources will likely be limited by the generated electron pulse quality in both the transverse and longitudinal (i.e., temporal) directions. In the spatial dimension orthogonal to the electron pulse propagation direction, a high quality electron beam requires a low normalized transverse rms emittance [10], commonly defined as $\varepsilon_T = \Delta x \Delta p_T / m_0 c$, where Δx is the transverse rms electron source size, Δp_T is the transverse rms momentum of the electrons, and m_0 is the free electron mass in vacuum. As this quantity is conserved in propagation through perfect electron optics [10], its value at the photocathode must be minimized, where reducing Δx is limited either by the incident laser focusing conditions or Child's Law [11]—two properties that are relatively material independent—leaving only the emitted electrons' Δp_T. For metal photocathodes, an expression for the transverse rms momentum has been analytically derived [12,13], $\Delta p_T = \sqrt{m_0(\hbar\omega - \phi)/3}$, where $\hbar\omega$ is the incident photon energy and ϕ is the work function of the metal. From this expression, which assumes electrons in a metal have the vacuum mass, it would appear that our only control over reducing ε_T is to minimize the maximum photoemission energy $\Delta E = \hbar\omega - \phi$ of the electrons [14]. In this Letter, we show that this is not the case, because the prior analyses [12,13] neglected the influence of the electron effective mass m^* in the metal on Δp_T. Nonetheless, a straightforward extension of these prior analyses illustrates the inherent dependency of Δp_T on m^*, which is verified by our experimental measurements of Δp_T on eight polycrystalline metal photocathodes: Ag, Be, Cr, Cu, Mo, Sn, Ta, and W.

To describe the complex process of photoemission, many have looked towards the works of Dowell [12] and Jensen [13], who have derived the same result for the transverse emittance of a photoemitted electron. In these analyses, the three-step model is used to describe photoemission, whereby (i) the electron absorbs the photon's energy, (ii) it is transported to the surface, and (iii) it is then transmitted outside of the metal. Dowell implies that the absorbed photon's energy adds to the total kinetic energy of the electron, so that the total momentum of the electron inside the metal p_{tot} becomes $\sqrt{2m_0(E + \hbar\omega)}$, where E is the total energy of the electron before its inelastic collision with the photon. For the electron to escape the metal, it requires a minimum momentum perpendicular to the surface of $p_z = \sqrt{2m_0(E_F + \phi)}$, where E_F is the Fermi energy, defining a maximal internal angle $\theta_{\text{int}}^{\max}$ for which the electron can still escape:

$$\cos\theta_{\text{int}}^{\max} = \frac{p_z}{p_{\text{tot}}} = \sqrt{\frac{E_F + \phi}{E + \hbar\omega}}. \tag{1}$$

In the low temperature limit ($T \to 0$ K), the expression for rms transverse momentum simplifies to

$$\langle p_T^2 \rangle = \frac{\int_{E_F+\phi-\hbar\omega}^{E_F} dE \int_{\cos\theta_{\text{int}}^{\max}}^{1} d(\cos\theta) \int_0^{2\pi} d\Phi\, p_T^2}{\int_{E_F+\phi-\hbar\omega}^{E_F} dE \int_{\cos\theta_{\text{int}}^{\max}}^{1} d(\cos\theta) \int_0^{2\pi} d\Phi}, \tag{2}$$

where $p_T = p_{\text{tot}} \sin\theta \cos\Phi = \sqrt{2m_0(E + \hbar\omega)} \sin\theta \cos\Phi$. After integration, Eq. (2) reduces analytically to [12,13]

$$\Delta p_T = \sqrt{m_0(\hbar\omega - \phi)/3}, \tag{3}$$

a strikingly simple result for a complex process.

In our approach, we assume that the absorbed photon energy $\hbar\omega$ excites the electron to a virtual state where it conserves its original momentum after the inelastic collision (the absorption); that is, the photon's momentum is negligible compared to that of the electron ($\hbar\omega/c \ll p_{\mathrm{tot}}$). Further, in our adaptation of Dowell's analysis [12], we consider an isotropic electron effective mass in the metal associated with the curvature of the electronic band in the vicinity of the Fermi energy

$$\frac{1}{m^*} = \frac{d^2E}{dp^2}\bigg|_{E=E_F},$$

which then modifies the expression for p_{tot}. This means that this virtual excited state maintains the energy-momentum dispersion of the energy band from which the electrons were photoexcited. These two adaptations to the analysis have the following effect: $\cos\theta_{\mathrm{int}}^{\mathrm{max}} = \sqrt{(E_F + \phi - \hbar\omega)/E}$ and $p_T = \sqrt{2m^*E}\sin\theta\cos\Phi$. As a result, for $m^* < m_0$, Eq. (3) becomes

$$\Delta p_T = \sqrt{\frac{m^*(\hbar\omega - \phi)}{3}}, \tag{4}$$

a similarly striking result, as remarkably, the two new assumptions analytically simplify to the same result with m^* in place of m_0. This is, of course, a direct consequence of the conservation of momentum parallel to the photocathode-vacuum interface, which limits the maximum external emission angle to $\sin^{-1}(\sqrt{m^*/m_0})$ [15], simply because for a given excess photoemission energy ΔE, $p_T^{\mathrm{max}} = \sqrt{2m^*\Delta E}$ so that $p_{z,\mathrm{ext}}^{\mathrm{max}} = \sqrt{2(m_0 - m^*)\Delta E}$ by energy conservation, and hence $\tan\theta_{\mathrm{ext}}^{\mathrm{max}} = \sqrt{m^*/(m_0 - m^*)}$. On the other hand, for $m^* > m_0$, $p_{z,\mathrm{ext}}^{\mathrm{max}}$ becomes imaginary for the maximum possible value of p_T, resulting in the reflection of the excited electron wave function back into the photocathode—in analogy to total internal reflection in optics. Only for $p_T \le \sqrt{2m_0\Delta E}$ can the electrons now be emitted, giving $\theta_{\mathrm{ext}}^{\mathrm{max}} = 90°$ and returning Eq. (4) as the valid expression for Δp_T.

In reality, electrons may have different effective masses along different crystal directions. However, the above approach should hold for the polycrystalline metal photocathodes employed in our experimental studies as they are effectively isotropic materials with an average m^* or, more specifically, an average effective mass parallel to the metal-vacuum interface.

In our studies, the transverse rms momentum Δp_T of electron pulses generated using a 20 kV laser-driven dc photoelectron gun has been determined for eight planar bulk polycrystalline elemental metal photocathodes at 300 K: Ag, Be, Cr, Cu, Mo, Sn, Ta, and W. The solenoid scan technique [10] is employed to measure the propagation properties of electron pulses and thereby extract their transverse rms momentum through simulation of the experiment using an extended analytical Gaussian (AG) electron pulse propagation model [16,17]. The 261 nm ($\hbar\omega = 4.75$ eV), p-polarized, ~4 ps duration, UV laser pulses incident on the metal photocathodes are produced by harmonic conversion of a diode-pumped, femtosecond Yb:KGW laser [18,19]. As shown in Fig. 1, after generation and acceleration in the dc gun, the electron pulses are directed down the axis of a pair of coupled large-aperture (6.35 mm-diameter) magnetic lenses to a YAG scintillator screen, which enables their integrated transverse pulse profile to be captured using a CCD camera as a function of the current in the magnetic lens coils. Armed with the knowledge that a magnetic lens current of 2.03 A focuses the electron beam onto the YAG scintillator, the experimental geometry (i.e., distances between column elements), and the fact that the strength of the magnetic lenses is proportional to the square of the current running through their coils [10], allows one to simulate quite accurately the measurement technique using our extended AG model, which now also includes relativistic corrections—although, in this case, the relativistic γ factor is only 1.04.

Figure 2 displays the results obtained using the solenoid scan technique for the polished planar Mo photocathode—a metal that does not readily oxidize and has a well characterized photoelectric work function [20,21]. The measured half width at $1/e$ maximum (HWe^{-1}M) electron beam spot size on the YAG scintillator clearly has the expected linear focusing (and defocusing) dependence on the square of the applied magnetic lens current (i.e., lens strength) with a focus at around 2.03 A. The observed variation of the HWe^{-1}M beam size with lens strength is readily simulated using the extended AG model of the experiment with just two free parameters: (i) the transverse rms momentum Δp_T of the beam, which determines its convergence (divergence), and (ii) the focal spot size. As the minimum focal spot size of ~150 μm is significantly greater than the ~50 μm "point spread function" of the YAG scintillator, the latter plays little role in the measurements. The fitted value of $0.20(\pm 0.01)(m_0\ \mathrm{eV})^{1/2}$ for Δp_T extracted using the simulation may be determined with an accuracy of typically better than 5%, provided sufficient

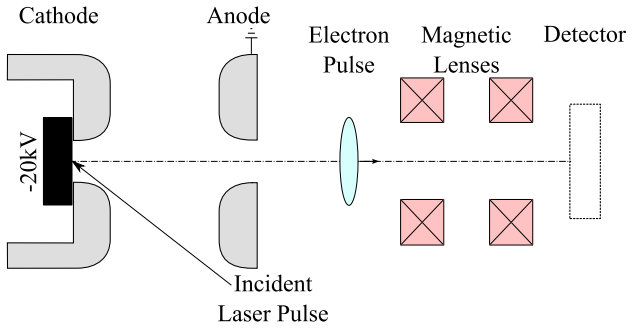

FIG. 1 (color online). The 20 kV dc electron gun and coupled magnetic lens geometry for Δp_T measurements.

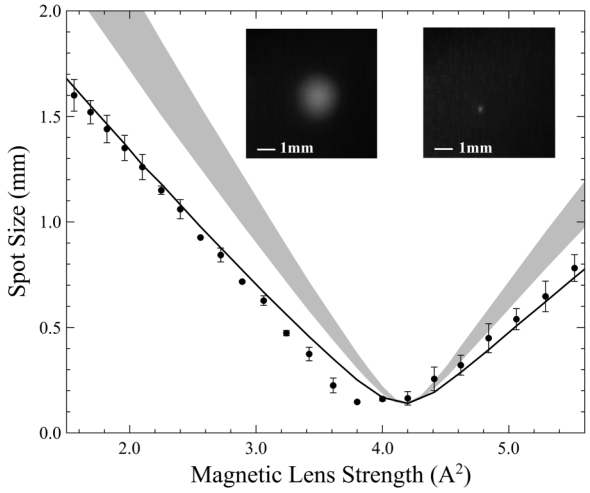

FIG. 2. The measured HWe^{-1}M spot size of the electron beam generated by a Mo photocathode at different lens strengths fitted using our AG model (solid curve). Also shown is the theoretical result based on Eq. (3) (shaded region) and two images of the electron beam spot captured by our CCD array at 1.45 and 2.05 A.

care is taken to ensure that (i) the electron beam propagates down the axis of the lens system to avoid astigmatism, and (ii) the intrapulse space charge effects are insignificant to ensure negligible beam degradation while the pulse propagates through the system. The latter condition is well satisfied since the experiment is run at low UV laser power and hence low electron pulse charge; we generate less than 1000 electrons/pulse from a $\sim$100 μm spot size on the photocathode using our $\sim$4 ps 261 nm UV laser pulse. This translates to a factor of $\sim$100 below the ''short-pulse'' Child's law limit [11] for our dc photogun, and simulations with the AG model indicate that the maximum $\sim 10^4$ C/m^3 accelerated pulse charge density is also 2 orders of magnitude below that required for space-charge effects to be observed in the experiment.

Also plotted in Fig. 2 is the expected range of the variation of the beam size with magnetic lens current for the value of the transverse rms momentum predicted for Mo by Eq. (3) [12,13], i.e., $\Delta p_T = 0.27(\pm 0.03)(m_0\ \mathrm{eV})^{1/2}$ using the same 150 micron focal spot size. Here, we have ignored the Schottky effect (only $\sim$30 meV in our case) and so have taken the work function ϕ of polycrystalline Mo to be 4.53($\pm$0.05) eV [20]: $\phi = 4.53$ eV for the (100) face (likely the most favored orientation for a body-centered cubic polycrystalline sample [21,22]) and $\phi = 4.55$ eV for the (111) face. The 4.95 eV work function for the (110) face is inaccessible to our 4.75 eV photon energy. The clear 30% disagreement between the prediction of Eq. (3) and our measurement of $\Delta p_T = 0.20(\pm 0.01) \times (m_0\ \mathrm{eV})^{1/2}$ for Mo can be explained by the electron effective mass analysis presented above. Specifically, cyclotron resonance measurements on Mo indicate an electron effective mass of about $0.35(\pm 0.05)m_0$ [23,24] in the (100) crystal plane, which, using Eq. (4), provides a value for Δp_T of between 0.13 and 0.19 $(m_0\ \mathrm{eV})^{1/2}$—in better agreement with our experimental determination.

TABLE I. Results from experiment and other relevant data. The work functions are given by Ref. [20] unless otherwise indicated or are photoelectric measurements unless otherwise indicated.

Metal	$\Delta p_{T,\mathrm{expt}}$ ($\sqrt{m_0\mathrm{eV}}$)	ϕ (eV)	m^*/m_0
Ag	0.235	4.64 (100)	0.95–1.01[a,b]
		4.52 (110)	
		4.74 (111)	
Be	0.225	3.92 (P)[c]	0.16–0.18[d]
Cr	0.155	4.5 (P)	0.20–0.40[e]
Cu	0.130	4.59 (100)	1.35–1.50[b,f]
		4.48 (110)	
		4.98 (111)	
Mo	0.200	4.53 (100)	0.30–0.40[g]
		4.95 (110)	
		4.55 (111)	
Sn	0.248	4.3 (P)[h]	0.23–0.42[i]
Ta	0.185	4.15 (100)[j]	0.70–0.90[k]
		4.80 (110)[j]	
		4.00 (111)[j]	
		4.55 (P)[l]	
W	0.150	4.63 (100)[m]	0.25–0.40[n]
		5.25 (110)[m]	
		4.47 (111)[m]	
		4.6 (P)	
Mg	0.330[o]	3.66 (P)[o]	0.16–0.36[p]

[a]Reference [25].
[b]Reference [26].
[c]Reference [27].
[d]Reference [28].
[e]Reference [29].
[f]Reference [30].
[g]References [23,24].
[h]Reference [31].
[i]Reference [32].
[j]Thermionic emission measurement.
[k]Reference [33].
[l]Reference [34].
[m]Field emission measurement.
[n]Reference [35].
[o]Reference [36].
[p]Reference [37].

In Table I, for all eight polycrystalline metal photocathodes, we provide the experimentally determined values of the transverse rms momentum $\Delta p_{T,\mathrm{expt}}$ together with literature values of both their work function ϕ and electron effective mass m^*. In many cases, ϕ is given for different crystal faces, although for Be, Cr, and Sn only polycrystalline (P) values are available [20,26,27]. The values for m^* mainly originate from cyclotron resonance and de Haas–van Alphen measurements [31,36,37]; however, for both Ag and Cu reliable values have been determined by optical techniques [38]. For several of the metal

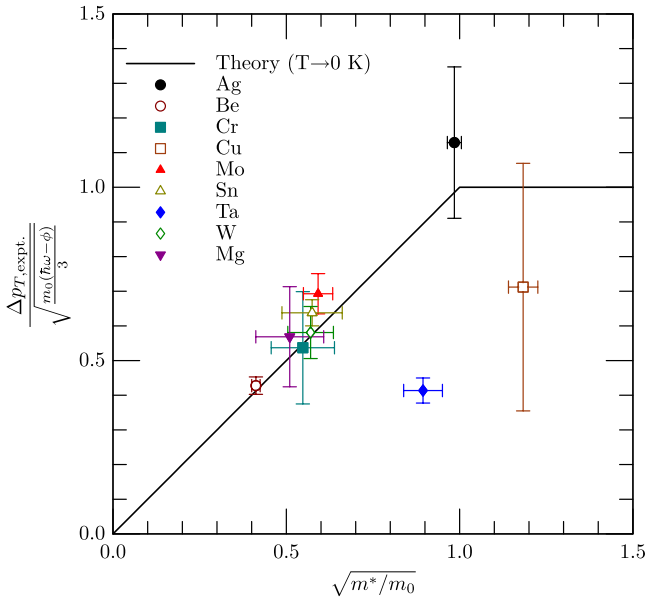

FIG. 3 (color online). Normalized $\Delta p_{T,\mathrm{expt}}$ vs $\sqrt{m^*/m_0}$ for nine metal photocathodes and the $T \to 0$ K theoretical curve based on Eq. (4). Data for Mg taken from Ref. [39].

photocathodes, specifically Ag, Cu, and Ta, care was taken to reduce the effect of surface oxidation in the solenoid scan measurements of Δp_T by polishing under propan-2-ol (to exclude oxygen) prior to rapid (> 5 min) insertion in to the dc gun. Also provided in Table I is the value of $\Delta p_{T,\mathrm{expt}}$ determined by X. J. Wang *et al.* [39] for a polycrystalline Mg photocathode irradiated by 266 nm UV radiation, for which $\phi \approx 3.66$ eV and $m^* \approx 0.26 m_0$ [40].

All of these measurements are plotted in Fig. 3 in a normalized form, $\Delta p_{T,\mathrm{expt}}/\sqrt{m_0(\hbar\omega - \phi)/3}$ against $\sqrt{m^*/m_0}$, in order to allow for a comparison with the analysis presented above, which is depicted by the solid line in the figure. Immediately evident is that the experimental results are in accord with our electron effective mass analysis, even though the analytical result of Eq. (3) was obtained in the low temperature ($T \to 0$ K) limit. This is consistent with the interpretation that a 300 K photocathode temperature should only affect Δp_T when the excess energy of photoemission $\hbar\omega$ is comparable to $k_B T$ [12,13], which is not the case for any of the studied metals. The exception to the agreement between $\Delta p_{T,\mathrm{expt}}$ and our effective mass analysis is Ta, for which complete agreement would require either $\phi \approx 4.6$ eV or $m^* \approx 0.15 m_0$. The latter appears much more likely; an accurate band structure calculation should then provide the reason for this surprisingly small value of Δp_T for Ta.

The uncertainties in Fig. 3 are determined primarily by those for m^* in the abscissa and ϕ in the ordinate, the error in determining Δp_T from the coil scans being negligible compared to that in the literature values of ϕ. This suggests that the use of a tunable UV laser system, for an *in situ* measurement of ϕ, would provide a reduced experimental uncertainty. However, ϕ is also a function of crystal orientation, which implies that an electron pulse from a polycrystalline photocathode is initially generated with a discrete set of transverse rms momenta—one for each different microcrystalline emission face. Further studies on the influence of m^* on Δp_T should, therefore, be performed using single-crystal metal photocathodes. Such future investigations can then also be compared to band structure calculations to determine, for example, the influence of anisotropy in the electron effective mass near the Fermi level.

In summary, our experimental investigations on planar polycrystalline metal photocathodes indicate that Δp_T is dependent upon the electron effective mass m^* near the Fermi level in the metal. In fact, an extension of prior analyses [12,13] shows that the transverse rms momentum should be written as $\Delta p_T = \sqrt{M(\hbar\omega - \phi)/3}$ for an isotropic material in the low temperature limit ($k_B T \ll \hbar\omega - \phi$), where $M = m^*$ for $m^* < m_0$ and $M = m_0$ for $m^* \geq m_0$. This theoretical formulation is shown to be consistent with our solenoid scan measurements of Δp_T. Through the use of suitable robust single-crystal metal photocathodes, this realization should lead to the future generation of electron pulses with significantly lower transverse rms emittance ε_T (i.e., higher brightness) to improve the performance of UTEMs, DTEMs, XFELs, and other next generation pulsed x-ray sources [41,42].

This work was supported by the Department of Energy (Contract No. DE-FG52-09NA29451). J. A. B. acknowledges the support of a Department of Education GAANN fellowship (Contract No. DED P200A070409).

*brickm2@uic.edu

[1] A. H. Zewail, Annu. Rev. Phys. Chem. **57**, **65** (2006).
[2] G. Sciaini and R. J. D. Miller, Rep. Prog. Phys. **74**, 096101 (2011).
[3] R. Srinivasan, V. A. Lobastov, C.-Y. Ruan, and A. H. Zewail, Helv. Chim. Acta **86**, 1761 (2003).
[4] W. E. King, G. H. Campbell, A. Frank, B. Reed, J. F. Schmerge, B. J. Siwick, B. C. Stuart, and P. M. Weber, J. Appl. Phys. **97**, 111101 (2005).
[5] W. E. King, M. R. Armstrong, O. Bostanjoglo, and B. W. Reed, in *Science of Microscopy*, edited by P. W. Hawkes and J. C. H. Spence (Springer, New York, 2007), pp. 406–444.
[6] G. H. Campbell, T. B. LaGrange, W. E. King, N. D. Browning, M. R. Armstrong, J. S. Kim, B. W. Reed, A. M. Frank, B. C. Stuart, W. J. DeHope, B. J. Pyke, R. M. Shuttlesworth, F. V. Hartemann, and D. J. Gibson, Microsc. Microanal. **12**, 1428 (2006).
[7] Y. Ding, A. Brachmann, F.-J. Decker, D. Dowell, P. Emma, J. Frisch, S. Gilevich, G. Hays, P. Hering, Z. Huang, R. Iverson, H. Loos, A. Miahnahri, H.-D. Nuhn, D. Ratner, J. Turner, J. Welch, W. White, and J. Wu, Phys. Rev. Lett. **102**, 254801 (2009).

[8] H. N. Chapman, A. Barty, M. J. Bogan, S. Boutet, M. Frank, S. P. Hau-Riege, S. Marchesini, B. W. Woods, S. Bajt, W. H. Benner, R. A. London, E. Plönjes, M. Kuhlmann, R. Treusch, S. Düsterer, T. Tschentscher, J. R. Schneider, E. Spiller, T. Möller, C. Bostedt, M. Hoener, D. A. Shapiro, K. O. Hodgson, D. van der Spoel, F. Burmeister, M. Bergh, C. Caleman, G. Huldt, M. M. Seibert, F. R. N. C. Maia, R. W. Lee, A. Szöke, N. Timneanu, and J. Hajdu, Nat. Phys. **2**, 839 (2006).
[9] Compact X-ray Light Source, Workshop PNNL-22145 (Pacific Northwest National Laboratory, Richland, Washington, 2012), http://www.emsl.pnl.gov/root/publications/docs/compact_xray.pdf.
[10] M. Reiser, *Theory and Design of Charged Particle Beams* (Wiley, New York, 2008).
[11] Á. Valfells, D. W. Feldman, M. Virgo, P. G. O'Shea, and Y. Y. Lau, Phys. Plasmas **9**, 2377 (2002).
[12] D. H. Dowell and J. F. Schmerge, Phys. Rev. ST Accel. Beams **12** (2009).
[13] K. L. Jensen, P. G. O'Shea, D. W. Feldman, and J. L. Shaw, J. Appl. Phys. **107**, 014903 (2010).
[14] C. P. Hauri, R. Ganter, F. Le Pimpec, A. Trisorio, C. Ruchert, and H. H. Braun, Phys. Rev. Lett. **104** (2010).
[15] Z. Liu, Y. Sun, P. Pianetta, and R. F. W. Pease, J. Vac. Sci. Technol. B **23**, 2758 (2005).
[16] A. M. Michalik and J. E. Sipe, J. Appl. Phys. **99**, 054908 (2006).
[17] J. A. Berger and W. A. Schroeder, J. Appl. Phys. **108**, 124905 (2010).
[18] J. A. Berger, B. L. Rickman, T. Li, A. W. Nicholls, and W. Andreas Schroeder, Appl. Phys. Lett. **101**, 194103 (2012).
[19] J. A. Berger, M. J. Greco, and W. A. Schroeder, Opt. Express **16**, 8629 (2008).
[20] J. Hölzl, F. K. Schulte, and H. Wagner, *Solid Surface Physics*, Springer Tracts in Modern Physics, Vol. 85 (Springer-Verlag, Berlin, 1979).
[21] I. L. Dillamore and W. T. Roberts, Metall. Rev. **10**, 271 (1965).
[22] D. Jacobson and A. Campbell, Metall. Trans. **2**, 3063 (1971).
[23] K. Dobson and A. Myers, Solid State Commun. **35**, 27 (1980).
[24] M. Surma, J. Magn. Magn. Mater. **11**, 56 (1979).
[25] D. G. Howard, Phys. Rev. **140**, A1705 (1965).
[26] M. M. Mann, Jr. and L. A. DuBridge, Phys. Rev. **51**, 120 (1937).
[27] M. Green, *Solid State Surface Science* (Marcel Dekker, Inc., New York, NY, 1969), Vol. 1.
[28] T. A. Kennedy and G. Seidel, Phys. Rev. B **6**, 3706 (1972).
[29] J. E. Graebner and J. A. Marcus, Phys. Rev. **175**, 659 (1968).
[30] E. Fawcett, Phys. Rev. **103**, 1582 (1956).
[31] G. Dresselhaus, A. Kip, and C. Kittel, Phys. Rev. **92**, 827 (1953).
[32] J. E. Craven, Phys. Rev. **182**, 693 (1969).
[33] A. Thorsen and T. Berlincourt, Phys. Rev. Lett. **7**, 244 (1961); L. L. Boyer, D. A. Papaconstantopoulos, and B. M. Klein, Phys. Rev. B **15**, 3685 (1977).
[34] J. L. Gumnick and D. W. Juenker, J. Appl. Phys. **31**, 102 (1960).
[35] R. F. Girvan, A. V. Gold, and R. A. Phillips, J. Phys. Chem. Solids **29**, 1485 (1968).
[36] C. Kittel, *Introduction to Solid State Physics* (Wiley, New York, 2005), 8th ed.
[37] D. Shoenberg, in *Progress in Low Temperature Physics*, edited by C. J. Gorter (North-Holland, Amsterdam, 1957). Vol. 2, pp. 226–265.
[38] P. B. Johnson and R. W. Christy, Phys. Rev. B **6**, 4370 (1972).
[39] X. J. Wang, M. Babzien, R. Malone, and Z. Wu, in *Proceedings of LINAC2002, Gyeongju, Korea, 2002* (Pohang Accelerator Laboratory, Pohang, Korea, 2002), pp. 142–144.
[40] D. A. Zych and T. G. Eck, Phys. Rev. B **1**, 4639 (1970).
[41] D. Dowell, I. Bazarov, B. Dunham, K. Harkay, C. Hernandez-Garcia, R. Legg, H. Padmore, T. Rao, J. Smedley, and W. Wan, Nucl. Instrum. Methods Phys. Res., Sect. A **622**, 685 (2010).
[42] K.-J. Kim, Y. Shvyd'ko, and S. Reiche, Phys. Rev. Lett. **100** (2008).